


RESEARCH ARTICLE

Brain atlas of the African mole-rat *Fukomys anselli*

Alexa Dollas¹ | Helmut H. A. Oelschläger² | Sabine Begall^{1,3} | Hynek Burda^{1,3} | Erich Pascal Malkemper^{1,4} 

¹Department of General Zoology, Faculty of Biology, University of Duisburg-Essen, Essen, Germany

²Department of Anatomy III (Dr. Senckenbergische Anatomie), Medical Faculty, Johann Wolfgang Goethe University, Frankfurt, Germany

³Department of Game Management and Wildlife Biology, Faculty of Forestry and Wood Sciences, Czech University of Life Sciences, Praha 6, Czech Republic

⁴Research Institute of Molecular Pathology (IMP), Vienna Biocenter (VBC), Campus-Vienna-Biocenter 1, Vienna 1030, Austria

Correspondence

Erich Pascal Malkemper, Research Institute of Molecular Pathology (IMP), Vienna Biocenter (VBC), Campus-Vienna-Biocenter 1, 1030 Vienna, Austria,
Email: pascal.malkemper@imp.ac.at

Abstract

African mole-rats are subterranean rodents that spend their whole life in underground burrow systems. They show a range of morphological and physiological adaptations to their ecotope, for instance severely reduced eyes and specialized somatosensory, olfactory, and auditory systems. These adaptations are also reflected in the accessory sensory pathways in the brain that process the input coming from the sensory organs. So far, a brain atlas was available only for the naked mole-rat (*Heterocephalus glaber*). The Ansell's mole-rat (*Fukomys anselli*) has been the subject of many investigations in various disciplines (ethology, sensory physiology, and anatomy) including magnetic orientation. It is therefore surprising that an atlas of the brain of this species was not available so far. Here, we present a comprehensive atlas of the Ansell's mole-rat brain based on Nissl and Klüver-Barrera stained sections. We identify and label 375 brain regions and discuss selected differences from the brain of the closely related naked mole-rat as well as from epigeic mammals (rat), with a particular focus on the auditory brainstem. This atlas can serve as a reference for future neuroanatomical investigations of subterranean mammals.

KEYWORDS

auditory system, magnetoreception, nervous system, neuroanatomy, Nissl, rodent, RRID: SCR_005910, RRID:SCR_014199, subterranean mammal

1 | INTRODUCTION

More than 250 rodent species spend their whole life underground in self-dug tunnel systems. With the exception of Antarctica and Australia, subterranean rodents can be found on all continents. African mole-rats (Bathergidae) are a family of strictly subterranean rodents endemic to sub-Saharan Africa that comprises six genera of small to medium sized (40–2000 g) species. At least 18–29 species of African mole-rats are currently recognized (Monadjem, Taylor, Denys, & Cotterill, 2015; Wilson, Mittermeier, Ruff, Martínez-Vilalta, & Cavallini, 2016).

African mole-rats share a common phenotype that reflects the selective pressures of their underground habitat. It includes a cylindrical body shape, elastic skin, a short tail and short fur, reduced pinnae, and enlarged extrabuccal incisors (reviewed in Begall, Burda, & Schleich, 2007; cf. Figure 1). Physiologically, these animals show a high tolerance to hypoxic and hypercapnic conditions (Chung, Dzal, Seow, Milsom, & Pamenter, 2016; Larson & Park, 2009; Nevo, 1999;

Park et al., 2017). Their sensory organs have also adapted to the dark and featureless underground environment (Burda, Bruns, & Müller, 1990). Eye size is much reduced and the visual acuity very low (Kott, Němec, Fremlová, Mazoch, & Šumbera, 2016; Němec et al., 2008; Peichl, Němec, & Burda, 2004). The visual capabilities are sufficient, however, for brightness discrimination (detection of opened burrows; Kott, Šumbera, & Němec, 2010; Němec, Cvejková, Burda, Benada, & Peichl, 2007; Wegner, Begall, & Burda, 2006a), and they might help (at least in the laboratory) entrainment to the photoperiod (de Vries, Oosthuizen, Sichilima, & Bennett, 2008). Hearing is restricted to the low-frequency range which propagates best in underground tunnel systems (Gerhardt, Henning, Begall, & Malkemper, 2017; Lange et al., 2007). The somatosensory system is generally well-developed (Catania & Remple, 2002) and the animals detect seismic cues that are used for communication and orientation (Mason & Narins, 2010). Olfaction is also well developed and plays an important role in foraging and the recognition of conspecifics (Heth et al., 2002; Heth & Todrank, 2007). Furthermore, several species of African mole-rats



FIGURE 1 Adult Ansell's mole-rat (*Fukomys anselli*). Note the prominent rhinarium, vibrissae, and incisors as well as the severely reduced eyes and external ears (photo by Sarah Maria Wilms) [Color figure can be viewed at wileyonlinelibrary.com]

have a magnetic sense, most likely to aid navigation in the dark (Burda, Marhold, Westenberger, Wiltshcko, & Wiltshcko, 1990; Malewski et al., 2018; Oliveriusová, Němec, Králová, & Sedláček, 2012).

Given the many physiological and sensory adaptations of African mole-rats, it is of interest to know how their brains differ from epigeic, that is, mostly surface-dwelling, rodent counterparts. Kruska and Steffen (2009) studied the gross anatomy and encephalization indices of brains of the genus *Fukomys*. Superficially, the brains look very much like other rodent brains and the encephalization index is similar to that of surface-dwelling rodents. Total neuron and glia cell numbers in African mole-rats conform to scaling rules established for other rodents (with the exception of the naked mole-rat, see below; Kverková et al., 2018). Immunohistochemical analysis of the cholinergic, putative catecholaminergic, and serotonergic neuron systems of two mole-rat species (*Cryptomys hottentotus pretoriae*, *Bathyergus suillus*) by Bhagwandin, Fuxe, Bennett, and Manger (2008), concluded in line with former studies that their brains, in principle, exhibit the same complement of homologous nuclei as in other rodents. The central olfactory system is well-developed, the olfactory bulbs and olfactory allocortex are larger (relative to brain size) in mole-rats than in rats (Kruska & Steffen, 2009). The somatosensory cortex of the naked mole-rat is significantly enlarged, occupying most of the areas that are visual in epigeic rodents, with an over-representation of the incisors (Catania & Remple, 2002; Henry, Remple, O'Riain, & Catania, 2006). As a consequence, the visual cortex is small in bathyergid mole-rats and also the subcortical visual pathways show particularly strong deviations from those in other rodents. The optic nerve and optic chiasm are extremely thin (Kruska & Steffen, 2009; Němec et al., 2007). The central areas involved in visual processing, such as the lateral geniculate body and the superficial layers of the superior colliculus are significantly reduced in bathyergid mole-rats compared to epigeic rodents (Němec et al., 2008; Němec, Burda, & Peichl, 2004). Strong neuronal activation (c-fos labeling) in the retina, suprachiasmatic nucleus, lateral geniculate body, olivary pretectal nucleus, retrosplenial cortex, and visual cortex in animals exposed to light for 1 hr, however, demonstrated that the visual system is functional (Oelschläger, Nakamura, Herzog, & Burda, 2000). This has been confirmed in behavioral experiments (Kott et al., 2016; Wegner et al., 2006a). C-fos labeling has also provided seminal evidence for a mole-rat magnetic sense by showing that changing magnetic fields activate areas of the superior colliculus and the rodent navigation circuit (Burger et al., 2010; Němec,

Altmann, Marhold, Burda, & Oelschläger, 2001). The brains of African mole-rats are further interesting with respect to the complexity of sociality in these animals (Kverková et al., 2018). Since the social systems occurring in this rodent family span the full range from strictly solitary (i.e. only one individual inhabits a burrow system outside of the mating season) to eusocial, a unique platform to study the neural correlates of social behavior and brain evolution is provided. Expression patterns of oxytocin receptors, vasopressin and its receptors, corticotropin-releasing factors as well as markers of adult neurogenesis have been related to sociality, social ranks, and mating systems (Amrein et al., 2014; Coen et al., 2015; Kalamatianos et al., 2010; Peragine, Simpson, Mooney, Lovern, & Holmes, 2014; Rosen, De Vries, Goldman, Goldman, & Forger, 2007; Valesky, Burda, Kaufmann, & Oelschläger, 2012).

Given the number of neuroanatomical studies in different mole-rat species and their significance for the understanding of mammalian adaptation to the subterranean habitat it is astonishing that only a single anatomical atlas of a mole-rat brain was available until now (Xiao, Levitt, & Buffenstein, 2006). Previous investigators of mole-rat brains had to rely on the brain atlas of the naked mole-rat (Xiao et al., 2006) in combination with atlases of the laboratory mouse (Paxinos, 2013) and the laboratory rat (Paxinos & Watson, 2013; Swanson, 2004). While the naked mole-rat probably is the most popular and most intensively studied mole-rat species (Sherman, Jarvis, & Alexander, 2017), it shows several traits not shared by its closest relatives, such as an extreme litter size, furlessness and poikilothermy (Kock, Ingram, Frabotta, Honeycutt, & Burda, 2006). Indeed, this species is so distinct from other African mole-rats that it has recently been proposed to constitute its own rodent family, Heterocephalidae (Patterson & Upham, 2014). Furthermore, the brain of the naked mole-rat has been shown to differ from other African mole-rat brains and general rodent brain scaling rules in that it is relatively smaller and has fewer neurons than expected for a rodent of its body size (Kverková et al., 2018). It is therefore likely that the naked mole-rat brain is not representative for subterranean mammals. The extent to which the neuroanatomy of the naked mole-rat differs from that of other subterranean rodents has not been investigated mainly because studies on brain anatomy of other mole-rats are scarce.

About half of the African mole-rat species belong to the genus *Fukomys*. Within this genus, one of the most studied species is the Ansell's mole-rat *Fukomys anselli* (previously called *Cryptomys anselli*, Kock et al., 2006). The Ansell's mole-rat is a medium-sized (50–120 g) mole-rat endemic to Zambia that digs large and highly complex underground tunnel systems of up to 2.8 km length (Šklíba et al., 2012). It is eusocial and lives in small family groups of about 10–15 animals composed of a single breeding pair and its nonreproductive offspring (Pätzenauerová, Šklíba, Bryja, & Šumbera, 2013). The animals feed on plant tubers and roots and only rarely leave their burrow system (Scharff & Grütjen, 1997). With an average life expectancy of 7–8 years, the animals are extremely long-lived (with a thus far recorded maximum life span of nearly 20 years) for a rodent of their body size and they show a unique bimodal aging pattern with reproductive animals aging considerably slower than nonbreeders (Dammann & Burda, 2006). The Ansell's mole-rat has been studied for many decades as a paradigm for sensory and ecophysiological

adaptations to the underground environment, the evolution of social systems, and animal navigation (reviewed in Begall et al., 2007). Notably, it was the first mammal for which a magnetic compass sense was convincingly proven and characterized (Burda, Marhold, et al., 1990; Burger et al., 2010; Marhold, Burda, Kreilos, & Wiltshko, 1997; Marhold, Wiltshko, & Burda, 1997; Němec et al., 2001; Thalau, Ritz, Burda, Wegner, & Wiltshko, 2006; Wegner, Begall, & Burda, 2006b).

Here, we present a comprehensive atlas of the brain of *Fukomys ansellii* based on Nissl and Klüver-Barrera stained sections. We identified and labeled 375 brain regions and discuss some similarities to and differences from those of other subterranean and epigeic rodents including the rat. This atlas can serve as a reference guide for future neuroanatomical and physiological studies of mole-rat brains.

2 | MATERIALS AND METHODS

This atlas is based on serial brain sections of altogether 17 individuals of Ansell's mole-rat. Table 1 gives an overview of the Ansell's mole-rat histological material used in this study. The animals were deeply anesthetized and then transcardially perfused with heparinized saline followed by fixation with 4% paraformaldehyde (PFA) in phosphate buffer. The perfused animals were decapitated and their brains carefully dissected and postfixed in PFA overnight. Paraffin sections (14 μm) and cryo-sections (60 μm) were prepared according to standard histological procedures (Němec et al., 2001).

The atlas plates display a selection of transverse (coronal) sections of 14 μm thickness at a regular spacing of 280 μm from two subadult individuals, C25 (female) and C26 (male, plate 381). In other words, every 20th section was stained with cresyl violet (Nissl), predominantly showing neuron somata including nuclei and nucleoli, and every 21st

section with a combination of cresyl violet and Luxol fast blue (Klüver-Barrera) showing both somata and fiber tracts. In addition, three intact Ansell's mole-rat brains were used for macroscopic documentation and description (Figure 2). Nissl-stained serial brain sections of 24 individuals of adult Wistar and Sprague-Dawley rats were included for comparisons.

We decided to show paraffin sections because their histological quality is superior to that of cryo-sections. Tissue shrinkage, however, is higher in paraffin sections which must be kept in mind when taking absolute measurements from the atlas plates presented. The plates are not fitted into a stereotaxic framework because all the slides mainly served for identification and interpretation of many Ansell's mole-rat brain structures investigated in several publications, for example, on the magnetic orientation of these animals (Burger et al., 2010; Němec et al., 2001).

To prepare the atlas plates, the serial sections of the two Ansell's mole-rat individuals C25 and C26 were scanned at 200 \times magnification with a microscopic slide scanner (Leica Aperio AT Turbo). The sections were aligned and optimized for tones and brightness in Photoshop (CC2017, Adobe) before they were reduced to 15% of their original size for the final 300 dpi plates. The identification of brain regions in the Ansell's mole-rat was based on detailed comparisons to rat brain sections along with a rat brain atlas (Paxinos & Watson, 2013), a mouse brain atlas (Paxinos, 2013), and a naked mole-rat brain atlas (Xiao et al., 2006). Cortical areas were identified based on cytoarchitecture.

For labeling of the anatomical structures, the principle of Paxinos and co-workers (Paxinos, 2013; Paxinos & Watson, 2013) was used. Lowercase letters indicate fiber tracts, white matter, recesses, and ventricles, while uppercase letters indicate nuclei and cortex (gray

TABLE 1 Available histological material from *Fukomys ansellii*

Individual (ID)	Sex	Age	Reproductive state	Body mass	Brain mass	Sectional plane	Type of sections	Thickness of sections
C25	Female	34 weeks	Subadult, nonreproductive	57 g	Unknown	Coronal	Paraffin	14 μm
C26	Male	26 weeks	Subadult, nonreproductive	52 g	Unknown	Coronal	Paraffin	14 μm
C9 CKA3-5	Female	16 weeks	Juvenile, nonreproductive	26 g	0.80 g	Coronal	Cryo	60 μm
C10 CKA3-2	Male	7 years	Adult, reproductive	94 g	1.26 g	Coronal	Cryo	60 μm
C11 CKA3-1	Female	11 years	Adult, reproductive	106 g	1.10 g	Coronal	Cryo	60 μm
C12 CKA3-4	Female	40 weeks	Subadult, nonreproductive	48 g	1.07 g	Coronal	Cryo	60 μm
C13 CKA3-6	Female	16 weeks	Juvenile, nonreproductive	14 g	0.73 g	Coronal	Cryo	60 μm
C14 CKA3-3	Female	2 years	Adult, nonreproductive	76 g	1.10 g	Coronal	Cryo	60 μm
FA23 6,931	Male	1 year	Adult	Unknown	1.10 g	None	None	None
FA47 1,455	Male	Unknown	Unknown	Unknown	1.15 g	None	None	None
FA34 2,472	Female	Unknown	Adult, reproductive	Unknown	1.18 g	None	None	None
C _L 291294	Female	Unknown	Unknown	49 g	Unknown	Coronal	Cryo	60 μm
C _D 291294	Female	Unknown	Unknown	48 g	Unknown	Coronal	Cryo	60 μm
C _L 060295	Male	Unknown	Unknown	55 g	Unknown	Coronal	Cryo	60 μm
C _D 060295	Female	Unknown	Unknown	51 g	Unknown	Coronal	Cryo	60 μm
C _L 220595	Male	Unknown	Unknown	57 g	Unknown	Coronal	Cryo	60 μm
C _D 220595	Male	Unknown	Unknown	55 g	Unknown	Coronal	Cryo	60 μm
C _L 190995	Male	Unknown	Unknown	71 g	Unknown	Coronal	Cryo	60 μm
C _L 100995	Female	Unknown	Unknown	62 g	Unknown	Sagittal	Cryo	60 μm
C _D 190995	Male	Unknown	Unknown	68 g	Unknown	Coronal	Cryo	60 μm

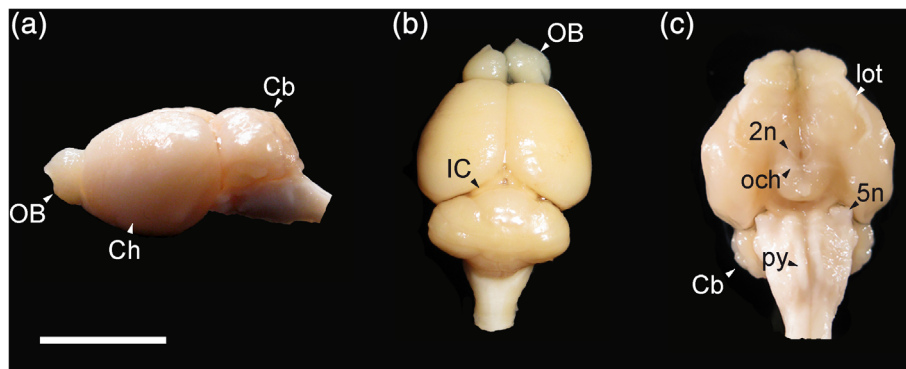


FIGURE 2 The brain of an adult Ansell's mole-rat specimen. One-year-old male. (a) Lateral aspect, (b) dorsal aspect, and (c) ventral aspect. Note the minute optic nerve (2n) and optic chiasm (och), the well-developed olfactory bulb (OB) and trigeminal nerve (5n), the large cerebral hemisphere (Ch), cerebellum (Cb) as well as the lateral olfactory tract (lot) and pyramidal tract (py). Scale bar: 1 cm [Color figure can be viewed at wileyonlinelibrary.com]

matter). This allows optimal orientation within the brain sections by keeping the information content of the plates high: Short abbreviations, adequate size of letters, and good discrimination of the anatomical structures.

3 | RESULTS AND DISCUSSION

The brain of *Fukomys anelli* (body mass: 50–120 g) resembles a rat brain but is less elongated in shape (Figure 2). With an average adult brain mass of 1.15 ± 0.06 g (mean \pm SD, $n = 6$) it is about two thirds the size of a rat brain (body mass: 300–500 g; Herculano-Houzel, 2009), but more than double the size of a naked mole-rat brain (body mass: 40–60 g; Kverková et al., 2018) or mouse brain (body mass: 15–40 g; Herculano-Houzel, 2009). The brain mass of the individuals used in the present study compares well to that reported for a similar sample size of Ansell's mole-rats in a recent study (Kverková et al., 2018). Macroscopic inspection of the Ansell's mole-rat brains (Figure 2) revealed several features related to the underground lifestyle, such as very thin optic nerves, a delicate optic chiasm but well-developed trigeminal nerves, ganglia, and branches (Figure 2).

The brain atlas contains 28 Cresyl violet stained coronal sections and 28 adjacent Klüver-Barrera stained sections that illustrate the myelinated fiber tracts. In the Cresyl violet sections of the brain stem, the cerebellum is omitted to allow higher magnification of details. Fiber tracts are indicated by lowercase abbreviations, brain nuclei by uppercase labeling. The approximate coronal plane of the section is shown in the schematic midsagittal inset in the upper left of each plate. All plates of this atlas can be viewed online on the Biolucida Server (<https://wiley.biolucida.net/images/?page=images&selectionType=collectionandselectionId=166>). A high-quality PDF will be provided by the authors upon request.

All major brain areas typical for rodents are found in the Ansell's mole-rat, in total we identified 375 different structures (Figure 4, Table 2 and online plates). Because no electrophysiological data are available for Ansell's mole-rats, we only annotated neocortical areas that were clearly identifiable based on cytoarchitecture. Whereas, in general, the shape and size of the brain structures in the Ansell's mole-rat are similar to other rodents, their topography is often rather different. This is reflected in the number of sections in the rat brain

atlas (Paxinos & Watson, 2013) that had to be consulted in order to identify and denominate the brain regions found on single brain sections of the Ansell's mole-rat. The rat-to-mole-rat ratios (calculated for each Ansell's mole-rat brain section) varied between 1:1 and 45:1 and were particularly high in the midbrain region. In part, this can be attributed to some deviation of the sectional angle in the rat and mole-rat brains. The marked structural differences in the topography of brain structures in the two species, however, emphasize the necessity for and value of a brain atlas for the Ansell's mole-rat.

Remarkable characteristics in the brain of the Ansell's mole-rat were found in the thalamus. The oval paracentral (OPC) as well as the paracentral thalamic nucleus (PC) were much more prominent in the

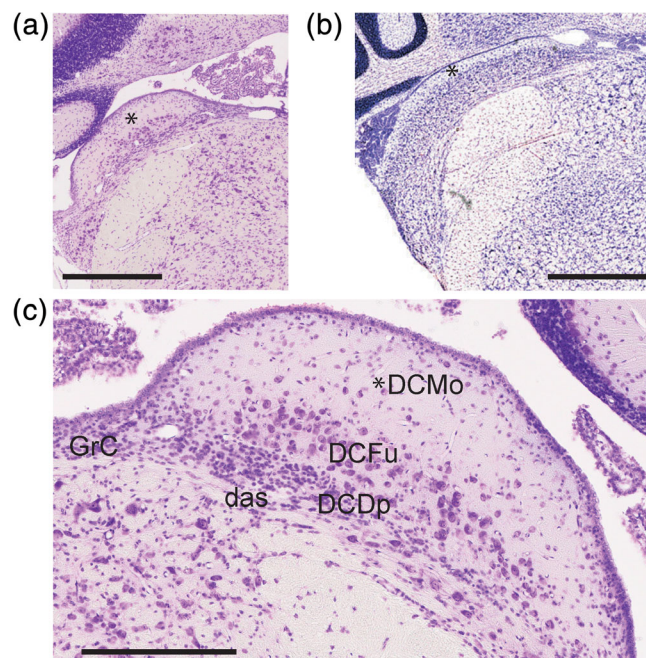


FIGURE 3 The dorsal cochlear nucleus of the Ansell's mole-rat in comparison to the laboratory rat. (a) The molecular layer of the mole-rat dorsal cochlear nucleus (asterisks) is large and more prominent than in (b) the rat. Scale bars: 600 μ m. (c) Higher magnification of the mole-rat dorsal cochlear nucleus shown in plate 940. Refer Table 2 for list of abbreviations. Scale bar: 300 μ m [Color figure can be viewed at wileyonlinelibrary.com]

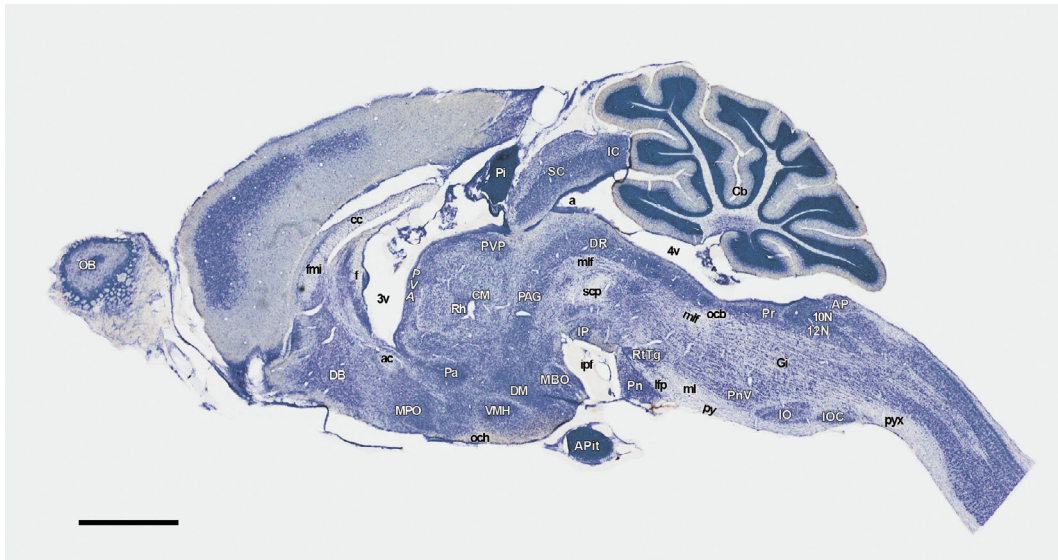


FIGURE 4 Nissl-stained mid-sagittal section of the brain of Ansell's mole-rat. All major structures seen in other rodent brains can be identified in the mole-rat brain. For further lettering see abbreviation list. Scale bar: 3 mm [Color figure can be viewed at wileyonlinelibrary.com]

Ansell's mole-rat (plate 620) than in the rat. Not much is known about the function of these nuclei but together with other intralaminar thalamic nuclei they are thought to be involved in processes related to awareness and arousal (Binder, Hirokawa, & Windhorst, 2009). The OPC has further been shown to receive noxious input from the masseter muscle, which is extremely well-developed in African mole-rats and provides them with one of the strongest bite forces (relative to body mass) in the animal kingdom (Cox & Faulkes, 2014; Sugiyo, Takemura, Dubner, & Ren, 2006; Van Daele, Herrel, & Adriaens, 2008). The lateral reticular nucleus in the medulla oblongata (LRT, plates 1,000–1,100) had both a larger rostrocaudal extension and a higher neuron density in the Ansell's mole-rat than in the rat. This nucleus is involved in locomotor-respiratory coordination (Ezure & Tanaka, 1997) and its larger size in the Ansell's mole-rat might be related to the specific respiratory conditions underground. Interestingly, the average respiratory rate of 36 breaths per minute in sleeping (not anesthetized) Ansell's mole-rats is very low for a rodent of their size (García Montero, Burda, & Begall, 2015). We were not able to identify the paratrigebral nucleus in the Ansell's mole-rat, a brain area involved in the integration of somatosensory reflexes related to nociceptive, respiratory, and cardiovascular mechanisms (Caous, de Sousa Buck, & Lindsey, 2001). This nucleus was also not demonstrated in the naked mole-rat (Xiao et al., 2006), a species for which reduced pain sensitivity has been reported (Omerbašić et al., 2016; Park et al., 2008).

The central auditory pathway of Ansell's mole-rats can be expected to show specific features because the hearing range is restricted to low frequencies and absolute sensitivities are rather low (Brückmann & Burda, 1997; Gerhardt et al., 2017). The hearing range comprises frequencies between 0.1 and 13 kHz and the cochlea is highly specialized in the Ansell's mole-rat (Gerhardt et al., 2017; Müller & Burda, 1989). Whereas there are more turns of the cochlea in this underground-dwelling species and the basilar membrane is slightly longer than in the rat, the overall spiral ganglion cell density is much lower (Müller, Laube, Burda, & Bruns, 1992) and half of the

cochlea is part of an acoustic fovea dedicated to the analysis of a narrow frequency band between 0.6 and 1 kHz. Taken together, these data indicate that the Ansell's mole-rat is anatomically adapted to low-frequency hearing in tunnels where these frequencies are found to propagate most efficiently (Heth, Frankenberg, & Nevo, 1986; Lange et al., 2007). Furthermore, sound localization is expected to be rather poor in strictly subterranean rodents as having been demonstrated for the naked mole-rat (*Heterocephalus glaber*; Heffner & Heffner, 1993), the blind mole rat (*Spalax ehrenbergi*; Heffner & Heffner, 1992) and the pocket gopher (*Geomys bursarius*; Heffner & Heffner, 1990).

How is this specialization in hearing reflected in the central ascending auditory pathway of the Ansell's mole-rat? In the blind mole rat, the pocket gopher and in the naked mole-rat all nuclei typical for the mammalian auditory pathway are present (Bronchti, Heil, Scheich, & Wollberg, 1989; Glendenning & Masterton, 1998; Heffner & Heffner, 1990, 1993), and the same is true for the Ansell's mole-rat. We did observe some features in nuclei of the auditory brainstem in the Ansell's mole-rat that might be related to a subterranean lifestyle and to low frequency hearing. The cochlear nucleus of Ansell's mole-rat, as the first central area receiving auditory information (plates 820–940), has a specialized dorsal subnucleus (DCN). In terrestrial mammals, the DCN is likely involved in the assessment and/or elimination of auditory “artifacts” caused by positional changes of the pinnae of an animal toward a sound source (Young & Davis, 2002; Oelschläger, 2008; Cozzi, Huggenberger, & Oelschläger, 2016, p. 286 for more information). Animals lacking moveable pinnae such as dolphins and seals tend to have a small DCN while it is prominent in cats, epigeic rodents, and bats (see Malkemper, Oelschläger, & Huggenberger, 2012). Although the Ansell's mole-rat lacks pinnae, the DCN is rather well-developed. While being less laminated than in the rat, the DCN of the Ansell's mole-rat is characterized by a thickened molecular layer (DCMo, plate 940, Figure 3) and an enlarged granular layer (GrC, plate 920). A prominent DCN has also been reported for the tunnel-dwelling mountain beaver (*Aplodontia rufa*) and the

TABLE 2 List of abbreviations

Abbreviations	long name of structure	Plate
10N	Dorsal motor nucleus of vagus	1,020–1,100, Figure 4
10n	Vagus nerve	1,040
11N	Accessory nerve nucleus	1,120
12N	Hypoglossal nucleus	1,000–1,100, Figure 4
12n	Hypoglossal nerve	1,040–1,100
2n	Optic nerve	440–460, Figure 2
3n	Oculomotor nerve	720
3N	Oculomotor nucleus	680–720
3v	Third ventricle	440–640, Figure 4
4N	Trochlear nucleus	700–740
4v	Fourth ventricle	780–1,040, Figure 4
5n	Trigeminal nerve	Figure 2
5N	Motor trigeminal nucleus	800–880
5Sol	Trigeminal-solitary transition zone	980–1,040
6N	Abducens nucleus	920–940
7n	Facial nerve	860–880, 920
7N	Facial nucleus	880–980
8cn	Cochlear root of the vestibulocochlear nerve	840–880
8vn	Vestibular root of the vestibulocochlear nerve	860–920
a	Aqueduct	620–760, Figure 4
ac	Anterior commissure	440–460, Figure 4
aca	Anterior commissure, anterior part	280–420
AcbC	Accumbens nucleus, core	340–400
AcbS	Accumbens nucleus, shell	340–400
aci	Anterior commissure, intrabulbar part	200–260
ACo	Anterior cortical amygdaloid nucleus	500–540
acp	Anterior commissure, posterior part	440
AD	Anterodorsal thalamic nucleus	480–520
AH	Anterior hypothalamic area	520–580
AHC	Anterior hypothalamic area, central part	500
AHP	Anterior hypothalamic area, posterior part	500
AM	Anteromedial thalamic nucleus	480–520
Amb	Ambiguous nucleus	1,060
AOB	Accessory olfactory bulb	180–200
AOD	Anterior olfactory nucleus, dorsal part	200–240
AOL	Anterior olfactory nucleus, lateral part	200–240
AOM	Anterior olfactory nucleus, medial part	200–240
AOV	Anterior olfactory nucleus, ventral part	200–240
AP	Area postrema	1,040–1,060, Figure 4
APit	Anterior lobe of the pituitary	700–780, Figure 4
APT	Anterior pretectal nucleus	600–680
Arc	Arcuate hypothalamic nucleus	620–640
AuD	Auditory cortex	480, 520, 620
AV	Anteroventral thalamic nucleus	480–520
azp	Azygous pericallosal artery	300–381
Bar	Barrington's nucleus	820–860
bic	Brachium of the inferior colliculus	680–720
BIC	Nucleus of the brachium of the IC	720
BLA	Basolateral amygdaloid nucleus, anterior part	460–580
BMA	Basomedial amygdaloid nucleus, anterior part	460–580
BMP	Basomedial amygdaloid nucleus, posterior part	580
C	Central canal	1,040–1,120

(Continues)

TABLE 2 (Continued)

Abbreviations	long name of structure	Plate
CA1	Field CA1 of the hippocampus	480–660
CA2	Field CA2 of the hippocampus	460–660
CA3	Field CA3 of the hippocampus	460–660
Cb	Cerebellum	Figures 2 and 4
CbN	Cerebellar nuclei	920
cc	Corpus callosum	360–520, Figure 4
Ce	Central amygdaloid nucleus	520–540
CeCv	Central cervical nucleus of the spinal cord	1,060
CG	Central gray	840–880
cg	Cingulum	300–600
Ch	Cerebral hemisphere	Figure 2
chp	Choroid plexus	360–580, 900–1,020
CIC	Central nucleus of the inferior colliculus	740–760
cic	Commissure of the inferior colliculus	700–740
CI	Caudal interstitial nucleus of the medial longitudinal fasciculus	300–480
CL	Centrolateral thalamic nucleus	500–580
CLi	Caudal linear nucleus of the raphe	740
CM	Central medial thalamic nucleus	480–580, Figure 4
CnF	Cuneiform nucleus	740–780
cp	Cerebral peduncle	580–740
CPu	Caudate putamen (striatum)	300–560
csc	Commissure of the superior colliculus	600–640
cu	Cuneate fasciculus	1,020–1,120
Cu	Cuneate nucleus	1,020–1,120
DA	Dorsal hypothalamic area	580
das	Dorsal acoustic stria	940, Figure 3
DB	Diagonal band	Figure 4
DCDp	Dorsal cochlear nucleus, deep core	900–940, Figure 3
DCFu	Dorsal cochlear nucleus, fusiform layer	920–940, Figure 3
DCIC	Dorsal cortex of the inferior colliculus	740–780
DCMo	Dorsal cochlear nucleus, molecular layer	900–940, Figure 3
Den	Dorsal endopiriform nucleus	360–560
dhc	Dorsal hippocampal commissure	460–540
Dk	Nucleus of Darkschewitsch	640–680
DLG	Dorsal lateral geniculate nucleus	600–640
DLL	Dorsal nucleus of the lateral lemniscus	760–780
dlo	Dorsal lateral olfactory tract	200
DM	Dorsomedial hypothalamic nucleus	640–660, Figure 4
DMC	Dorsomedial hypothalamic nucleus, compact part	620
DMD	Dorsomedial hypothalamic nucleus, dorsal part	600–620
DMTg	Dorsomedial tegmental area	800–840
DMV	Dorsomedial hypothalamic nucleus, ventral part	620
DpG	Deep gray layer of the SC	680
DpWh	Deep white layer of the SC	680
DR	Dorsal raphe nucleus	740–820, Figure 4
DS	Dorsal subiculum	540–580
dsc	Dorsal spinocerebellar tract	980–1,080
DTg	Dorsal tegmental nucleus	780–840
dtgx	Dorsal tegmental decussation	700
DTT1	Dorsal tenia tecta layer 1	280–320

(Continues)

TABLE 2 (Continued)

Abbreviations	long name of structure	Plate
DTT2	Dorsal tenia tecta layer 2	280–320
E	Ependyma and subependymal layer	100–180
ec	External capsule	300–620
ECIC	External cortex of the inferior colliculus	740–780
Ect	Ectorhinal cortex	520–580
ECu	External cuneate nucleus	1,000–1,060
EGP	External part of globus pallidus	460
eml	External medullary lamina	500–580
ep	Olfactory epithelium	20
EP	Entopeduncular nucleus	520–560
EPI	External plexiform layer of the olfactory bulb	20–200
EW	Edinger-Westphal nucleus	680–700
F	Fornix	420–700, Figure 4
FC	Fasciola cinereum	480
fi	Fimbria of the hippocampus	440–580
fmi	Forceps minor of the corpus callosum	280–340, Figure 4
fmj	Forceps major of the corpus callosum	540–720
fr	Fasciculus retroflexus	480–680
g7	Genu of the facial nerve	880–920
Ge5	Gelatinous layer of the caudal spinal trigeminal nucleus	1,080–1,120
Gi	Gigantocellular reticular nucleus	900–1,040, Figure 4
GiA	Gigantocellular reticular nucleus, alpha part	900
GiV	Gigantocellular reticular nucleus, ventral part	980
Gl	Glomerular layer of the olfactory bulb	20–200
GP	Globus pallidus	480–520
gr	Gracile fasciculus	1,080–1,120
Gr	Gracile nucleus	1,040–1,100
GrC	Granule cell layer of cochlear nuclei	820–940, Figure 3
GrDG	Granular layer of the dentate gyrus	460–620
hbc	Habenular commissure	560
HDB	Nucleus of the horizontal limb of the diagonal band	360–480
I	Intercalated nuclei of the amygdala	480–580
I8	Interstitial nucleus of the vestibulocochlear nerve	840–920
IAD	Interanterodorsal thalamic nucleus	480
IAM	Interanteromedial thalamic nucleus	500
IB	Interstitial nucleus of the medulla	1,100–1,120
IC	Inferior colliculus	720–780, Figures 2, 4
ic	Internal capsule	420–560
ICj	Islands of Calleja	300–340
ICjm	Islands of Calleja, major island	360–381
icp	Inferior cerebellar peduncle (restiform body)	880–1,020
IEn	Intermediate endopiriform nucleus	360–460
IG	Indusium griseum	340–480
IGL	Intergeniculate leaf	600–640
ILL	Intermediate nucleus of the lateral lemniscus	760–800
iml	Internal medullary lamina	480–500
InC	Interstitial nucleus of Cajal	700
InGi	Inner sublayer of the intermediate gray layer superior colliculus	680

(Continues)

TABLE 2 (Continued)

Abbreviations	long name of structure	Plate
InGo	Outer sublayer of the intermediate gray layer superior colliculus	680
INS	Insular cortex	480
InWh	Intermediate white layer of the SC	680
IO	Inferior olivary nucleus	980–1,080, Figure 4
IOA	Inferior olive, subnucleus A of medial nucleus	1,020–1,060
IOB	Inferior olive, subnucleus B of medial nucleus	1,000–1,060
IOBe	Inferior olive, beta subnucleus	1,060
IOC	Inferior olive, subnucleus C of medial nucleus	1,020–1,060, Figure 4
IOD	Inferior olive, dorsal nucleus	1,000–1,020
IOK	Inferior olive, cap of Kooy of the medial nucleus	1,060
IOPr	Inferior olive, principal nucleus	1,000
IP	Interpeduncular nucleus	700–760, Figure 4
ipf	Interpeduncular fossa	700, Figure 4
IPI	Internal plexiform layer of the olfactory bulb	40–200
IRt	Intermediate reticular nucleus	880–1,120
isRt	Isthmic reticular formation	740–760
KF	Kölliker-fuse nucleus	800
LaDL	Lateral amygdaloid nucleus, dorsolateral part	520–580
LC	Locus coeruleus	860
Ld	Lambdoid septal zone	400
LD	Laterodorsal thalamic nucleus	520–560
LDB	Lateral nucleus of the diagonal band	440–480
LDTg	Laterodorsal tegmental nucleus	780–820
LDTgV	Laterodorsal tegmental nucleus, ventral part	780–820
lfp	Longitudinal fasciculus of the pons	760–820, Figure 4
LH	Lateral hypothalamic area	560
LHb	Lateral habenular nucleus	500–560
ll	Lateral lemniscus	760–800
LM	Lateral mammillary nucleus	680
lo	Lateral olfactory tract	200–400
LOT	Nucleus of the lateral olfactory tract	480–500
LP	Lateral posterior thalamic nucleus	560–580
LPB	Lateral parabrachial nucleus	800–860
LPMC	Lateral posterior thalamic nucleus, mediocaudal part	660
LPO	Lateral preoptic area	480
lr4v	Lateral recess of the 4th ventricle	900–1,020
LRt	Lateral reticular nucleus	1,000–1,100
LSD	Lateral septal nucleus, dorsal part	360–420
LSI	Lateral septal nucleus, intermediate part	360–420
LSO	Lateral superior olive	820–860
LSS	Lateral stripe of the striatum	360–420
LSV	Lateral septal nucleus, ventral part	360–420
Lth	Lithoid nucleus	600–640
Lv	Lateral ventricle	300–620
LVe	Lateral vestibular nucleus	880–920
M	Motor cortex	520
M1	Primary motor cortex	480
M2	Secondary motor cortex	480
m5	Motor root of the trigeminal nerve	740–800
MBO	Mammillary body	Figure 4

(Continues)

TABLE 2 (Continued)

Abbreviations	long name of structure	Plate
mcp	Middle cerebellar peduncle	740–860
MCPC	Magnocellular nucleus of the posterior commissure	640
MD	Mediodorsal thalamic nucleus	480–580
MdD	Medullary reticular nucleus, dorsal part	1,060–1,120
mDR	Dorsal raphe nucleus	720
MdV	Medullary reticular nucleus, ventral part	1,060–1,120
ME	Median eminence	580
Me5	Mesencephalic trigeminal nucleus	720–860
me5	Mesencephalic trigeminal tract	800–860
MePD	Medial amygdaloid nucleus, posterodorsal part	520–560
MePV	Medial amygdaloid nucleus, posteroventral part	520–560
mfb	Medial forebrain bundle	540–560
MG	Medial geniculate nucleus	660–700
MHb	Medial habenular nucleus	480–580
Mi	Mitral cell layer of the olfactory bulb	40–200
ml	Medial lemniscus	540–1,080, Figure 4
mlf	Medial longitudinal fasciculus	680–1,120, Figure 4
Mlx	Medial lemniscus decussation	1,040–1,080
MM	Medial mammillary nucleus, medial part	700
MnA	Median accessory nucleus of the medulla	1,100–1,120
MnR	Median raphe nucleus	780–820
MoDG	Molecular layer of the dentate gyrus	460–620
MPA	Medial preoptic area	480
MPB	Medial parabrachial nucleus	840–860
MPL	Medial paralemniscial nucleus	800–820
MPO	Medial preoptic nucleus	460
MPT	Medial pretectal nucleus	620
MRe	Mammillary recess of the 3rd ventricle	660–700
mRt	Mesencephalic reticular formation	680–720
MS	Medial septal nucleus	360–400
MSO	Medial superior olive	840–880
mt	Mammillothalamic tract	460–680
MTu	Medial tuberal nucleus	620
MVe	Medial vestibular nucleus	880–1,020
Mx	Matrix region of the medulla	960–1,060
ns	Nigrostriatal bundle	580
Nv	Navicular nucleus of the basal forebrain	300–340
OB	Olfactory bulb	Figures 2, 4
Obex	Obex	1,080
oc	Olivocerebellar tract	960–1,020
ocb	Olivocochlear bundle	920, Figure 4
och	Optic chiasm	500–560, Figures 2, 4
ON	Olfactory nerve layer	60–160
OPC	Oval paracentral thalamic nucleus	620
OPT	Olivary pretectal nucleus	600–620
opt	Optic tract	520–600
Or	Oriens layer of the hippocampus	480–580
OT	Nucleus of the optic tract	600–620
ov	Olfactory ventricle (olfactory part of lateral ventricle)	200–300
Pa	Paraventricular hypothalamic nucleus	480–540, Figure 4

(Continues)

TABLE 2 (Continued)

Abbreviations	long name of structure	Plate
PAG	Periaqueductal gray	620–760, Figure 4
PBP	Parabrachial pigmented nucleus of the VTA	700–720
PC	Paracentral thalamic nucleus	520–620
pc	Posterior commissure	600–640
PCRt	Parvicellular reticular nucleus	880–1,040
Pe	Periventricular hypothalamic nucleus	520–540
PeF	Perifornical nucleus	600–620
PH	Posterior hypothalamic nucleus	640–680
Pi	Pineal gland	580–620, Figure 4
pim	Pia mater	180
Pir	Piriform cortex	280–620
pire	Pineal recess	600
PLH	Peduncular part of lateral hypothalamus	500–660
pm	Principal mammillary tract	700
Pn	Pontine nuclei	760–820, Figure 4
PnC	Pontine reticular nucleus, caudal part	820–880
PnO	Pontine reticular nucleus, oral part	740–800
PnV	Pontine reticular nucleus, ventral part	820–860, Figure 4
Po	Posterior thalamic nuclear group	540–660
PoDG	Polymorph layer of the dentate gyrus	500–620
PP	Peripeduncular nucleus	660
PPit	Posterior lobe of pituitary	640–780
Pr	Prepositus nucleus	900–1,000, Figure 4
PR	Prerubral field	660–680
Pr5	Principal sensory trigeminal nucleus	800–880
PrC	Precommissural nucleus	600
PrG	Pregeniculate nucleus of the prethalamus	600–640
PT	Paratenial thalamic nucleus	480
PTe	Paraterete nucleus	600
PTg	Pedunculo-pontine tegmental nucleus	760
PV	Paraventricular thalamic nucleus	500–600
PVA	Paraventricular thalamic nucleus, anterior part	460–480, Figure 4
PVG	Periventricular gray	600
PVP	Paraventricular thalamic nucleus, posterior part	Figure 4
Py	Pyramidal cell layer of the hippocampus	480–620
py	Pyramidal tract	840–1,100, Figures 2, 4
pyx	Pyramidal decussation	1,100–1,120, Figure 4
R	Red nucleus	700–720
Re	Reuniens thalamic nucleus	480–580
REth	Retroethmoid nucleus	660
rf	Rhinal fissure	200–680
Rh	Rhomboid thalamic nucleus	520–580, Figure 4
RIP	Raphe interpositus nucleus	880
RIs	Retroisthmus nucleus	760
RLi	Rostral linear nucleus of the raphe	700
RMg	Raphe magnus nucleus	820–960
RML	Supramammillary nucleus, lateral part	700
RMM	Supramammillary nucleus, medial part	680
RMS	Rostral migratory stream	260–320
Ro	Nucleus of roller	980–1,020
ROb	Raphe obscurus nucleus	960–1,040

(Continues)

TABLE 2 (Continued)

Abbreviations	long name of structure	Plate
RPa	Raphe pallidus nucleus	980–1,060
RPC	Red nucleus, parvocellular part	680
RPF	Retroparafascicular nucleus	620
RRF	Retrorubral field	740
rs	Rubrospinal tract	800–1,120
RS	Retrosplenial cortex	580
Rt	Reticular thalamic nucleus	480–600
RtTg	Reticulotegmental nucleus of the pons	780–840, Figure 4
S	Somatosensory cortex	480, 520, 580
s5	Sensory root of the trigeminal nerve	740–880
Sag	Sagulum nucleus	760–780
SC	Superior colliculus	640–720, Figure 4
SCh	Suprachiasmatic nucleus	520–540
SCO	Subcommissural organ	600
scp	Superior cerebellar peduncle (brachium conjunctivum)	680–900, Figure 4
Shi	Septohippocampal nucleus	360–420
SHy	Septohypothalamic nucleus	420
sm	Stria medullaris of the thalamus	480–540
SMV	Superior medullary velum	820–880
SN	Substantia nigra	660–740
SO	Supraoptic nucleus	520–540
Sol	Nucleus of the solitary tract	940–1,120
sol	Solitary tract	980–1,100
sox	Supraoptic decussation	580
sp5	Spinal trigeminal tract	900–1,120
Sp5C	Spinal trigeminal nucleus, caudal part	1,060–1,120
Sp5I	Spinal trigeminal nucleus, interpolar part	960–1,060
Sp5O	Spinal trigeminal nucleus, oral part	900–960
SPTg	Subpeduncular tegmental nucleus	780
SpVe	Spinal vestibular nucleus	940–1,020
ST	Bed nucleus of the stria terminalis	420–480
st	Stria terminalis	460–560
STh	Subthalamic nucleus	600–660
STM	Bed nucleus of the stria terminalis, medial division	440
str	Superior thalamic radiation	600
Sub	Submedial thalamic nucleus	520–580
SubB	Subbrachial nucleus	680–700
SubC	Subcoeruleus nucleus	820–860
SubCA	Subcoeruleus nucleus, alpha part	820–860
SuL	Supralemniscal nucleus	760
SuVe	Superior vestibular nucleus	900
tfp	Transverse fibers of the pons	760–820
TGa	Terminal ganglion	20–40
ts	Tectospinal tract	760–800, 980–1,120
TS	Triangular septal nucleus	420
tth	Trigeminothalamic tract	700–820
Tu	Olfactory tubercle	320–420
TuLH	Tuberal region of lateral hypothalamus	520–620
tz	Trapezoid body	800–920
Tz	Nucleus of the trapezoid body	840–880

(Continues)

TABLE 2 (Continued)

Abbreviations	long name of structure	Plate
V	Visual cortex	620
VA	Ventral anterior thalamic nucleus	480–520
VCA	Ventral cochlear nucleus, anterior part	840–900
VCP	Ventral cochlear nucleus, posterior part	900–940
VDB	Nucleus of the vertical limb of the diagonal band	360–400
VL	Ventrolateral thalamic nucleus	500–560
vlh	Ventrolateral hypothalamic tract	500
VLL	Ventral nucleus of the lateral lemniscus	780–800
VM	Ventromedial thalamic nucleus	520–580
VMH	Ventromedial hypothalamic nucleus	500–620, Figure 4
VMPO	Ventromedial preoptic nucleus	480–500
VP	Ventral pallidum	320
VPL	Ventral posterolateral thalamic nucleus	520–640
VPM	Ventral posteromedial thalamic nucleus	540–640
VPPC	Ventral posterior nucleus of the thalamus, parvicellular part	620
VRe	Ventral reuniens thalamic nucleus	500–560
vsc	Ventral spinocerebellar tract	800–840, 980–1,120
VTA	Ventral tegmental area	680
VTg	Ventral tegmental nucleus	760
VTT	Ventral tenia tecta	240–280
X	Nucleus X	920–980
xscp	Decussation of the superior cerebellar peduncle	720–760
Z	Nucleus Z	1,020
ZI	Zona incerta	520–640

subterranean pocket gopher (Godfrey et al., 2016). In these species, the DCN amounts to more than 60% (pocket gopher) or almost 90% (mountain beaver) of the total cochlear nucleus volume (cat: 35%; Osen, 1969). Godfrey et al. (2016) interpreted these features of the DCN as possible adaptations facilitating the integration of somatosensory and auditory stimuli in the underground habitat which is in line with the interpretation of the dorsal cochlear nucleus in mammals, generally (see also Malmierca, 2015). The granule cells of the DCN receive direct input from many sources including the trigeminal somatosensory system and this information is likely processed in the molecular layer (Young & Davis, 2002). These layers in the Ansell's mole-rat might fulfill a similar function which is likely related to the somatosensory system but unrelated to pinna movements and sound localization. Godfrey et al. (2016) were puzzled by the fact that the naked-mole rat DCN did not show the “hypertrophic” features seen in other tunnel-dwelling rodents like the mountain beaver or the pocket gopher but resembled more the DCN of epigeic species. It did not show thickened molecular and granular layers and the relative size of the naked mole-rat DCN was similar to the DCN of the cat. They discussed the special situation in the naked mole-rat as a possible consequence of the social life-style of this species. Our data, however, do not support this idea because the Ansell's mole-rat also lives in social groups and its DCN shows the above-mentioned “hypertrophic” situation. We speculate that the pronounced granular and molecular regions of the DCN in the Ansell's mole-rat indeed may reflect an adaptation to the underground habitat and that the naked mole-rat is

an exception that shows signs of “degeneration” in its central auditory pathway as already proposed for the auditory periphery (Mason, Cornwall, & Smith, 2016). Neuroanatomical studies of more subterranean species will hopefully test this hypothesis.

Another nucleus of the auditory brainstem that shows features of low-frequency adaptations in the Ansell's mole-rat is the superior olive. The medial superior olive (MSO, plates 840–880), which is involved in the localization of low-frequency sounds in other mammals (Grothe, Pecka, & McAlpine, 2010), appears more differentiated in the Ansell's mole-rat than the lateral superior olive (LSO, plates 820–860) which is responsible for high frequency sound localization (Grothe et al., 2010). The LSO has also been reported as poorly differentiated in the blind mole rat (Bronchti et al., 1989) and as indistinct in the naked mole-rat (Heffner & Heffner, 1993; but see Gessele, Garcia-Pino, Omerbašić, Park, & Koch, 2016). Interestingly, all nuclei of the naked mole-rat's binaural auditory brainstem lack HCN1 channels that are necessary for fast integration times of interaural intensity differences which might explain the poor sound localization (Geselle et al., 2016). Collectively, the auditory pathway of the Ansell's mole-rat shows features found in other subterranean rodents that might represent adaptations to burrow acoustics. It must be noted here, however, that we present qualitative observations that should be quantitatively tested in further studies.

To summarize, we present an atlas that gives a good overview on brain organization in the Ansell's mole-rat together with many details needed for successful experimental neuroanatomical and physiological

work in this species. The atlas can also serve as a basis and background material for in-depth analyses concerning evolutionary processes leading to such exotic animals as the Ansell's mole-rat. We hope that the atlas may thus stimulate new questions and answers for promising investigations in the future.

ACKNOWLEDGMENTS

The authors thank U. Buckpesch-Heberer who delivered a first attempt to visualize the brain of *Fukomys anelli* and J.G. Veening, M. Nakamura, P. Němec, M. Herzog, S.G. Veitengruber, and S. Lohfink-Schumm for the preparation of the microslide series of brains used for this atlas. Finally, the authors thank two anonymous reviewers for comments that significantly improved this manuscript.

CONFLICT OF INTEREST

The authors declare no competing financial interests.

AUTHOR CONTRIBUTION

All authors had full access to all the data in the study and take responsibility for the integrity of the data and the accuracy of the data analysis. Study design: HHAO, EPM. Data acquisition: AD. Analysis and interpretation of data: AD, HHAO, SB, HB, EPM. Writing of the manuscript: AD, HHAO, SB, HB, EPM.

ORCID

Erich Pascal Malkemper  <https://orcid.org/0000-0003-1099-0119>

REFERENCES

- Amrein, I., Becker, A. S., Engler, S., Huang, S.-H., Müller, J., Slomianka, L., & Oosthuizen, M. K. (2014). Adult neurogenesis and its anatomical context in the hippocampus of three mole-rat species. *Frontiers in Neuroanatomy*, 8(39), 1–11.
- Begall, S., Burda, H., & Schleich, C. E. (Eds.). (2007). *Subterranean rodents: News from underground*. Heidelberg: Springer.
- Bhagwandin, A., Fuxe, K., Bennett, N. C., & Manger, P. R. (2008). Nuclear organization and morphology of cholinergic, putative catecholaminergic and serotonergic neurons in the brains of two species of African mole-rat. *Journal of Chemical Neuroanatomy*, 35(4), 371–387.
- Binder, M. D., Hirokawa, N., & Windhorst, U. (2009). *Encyclopedia of neuroscience*. Heidelberg: Springer.
- Bronchti, G., Heil, P., Scheich, H., & Wollberg, Z. (1989). Auditory pathway and auditory activation of primary visual targets in the blind mole-rat (*Spalax ehrenbergi*): I. 2-Deoxyglucose study of subcortical centers. *The Journal of Comparative Neurology*, 284, 253–274.
- Brückmann, G., & Burda, H. (1997). Hearing in blind subterranean Zambian mole-rats (*Cryptomys* sp.): Collective behavioural audiogram in a highly social rodent. *Journal of Comparative Physiology A: Neuroethology, Sensory, Neural, and Behavioral Physiology*, 181(1), 83–88.
- Burda, H., Bruns, V., & Müller, M. (1990). Sensory adaptations in subterranean mammals. In E. Nevo & O. A. Reig (Eds.), *Evolution of subterranean mammals at the organismal and molecular levels—Progress in clinical and biological research* (pp. 269–293). New York: Alan R. Liss Inc. Publishers.
- Burda, H., Marhold, S., Westenberger, T., Wiltschko, R., & Wiltschko, W. (1990). Evidence for magnetic compass orientation in the subterranean rodent *Cryptomys hottentotus* (Bathyergidae). *Experientia*, 46, 528–530.
- Burger, T., Lucová, M., Moritz, R. E., Oelschläger, H. H. A., Druga, R., Burda, H., ... Němec, P. (2010). Changing and shielded magnetic fields suppress c-Fos expression in the navigation circuit: Input from the magnetosensory system contributes to the internal representation of space in a subterranean rodent. *Journal of the Royal Society Interface*, 7(50), 1275–1292.
- Caous, C. A., de Sousa Buck, H., & Lindsey, C. J. (2001). Neuronal connections of the paratrigeminal nucleus: A topographic analysis of neurons projecting to bulbar, pontine and thalamic nuclei related to cardiovascular, respiratory and sensory functions. *Autonomic Neuroscience*, 94(1–2), 14–24.
- Catania, K. C., & Remple, M. S. (2002). Somatosensory cortex dominated by the representation of teeth in the naked mole-rat brain. *Proceedings of the National Academy of Sciences of the United States of America*, 99(8), 5692–5697.
- Chung, D., Dzal, Y. A., Seow, A., Milsom, W. K., & Pamentier, M. E. (2016). Naked mole rats exhibit metabolic but not ventilatory plasticity following chronic sustained hypoxia. *Proceedings of the Royal Society B: Biological Sciences*, 283(1827), 20160216.
- Coen, C. W., Kalamatianos, T., Oosthuizen, M. K., Poorun, R., Faulkes, C. G., & Bennett, N. C. (2015). Sociality and the telencephalic distribution of corticotrophin-releasing factor, urocortin 3, and binding sites for CRF type 1 and type 2 receptors: A comparative study of eusocial naked mole-rats and solitary cape mole-rats. *The Journal of Comparative Neurology*, 523(16), 2344–2371.
- Cox, P. G., & Faulkes, C. G. (2014). Digital dissection of the masticatory muscles of the naked mole-rat, *Heterocephalus glaber* (Mammalia, Rodentia). *PeerJ*, 2, e448.
- Cozzi, B., Huggenberger, S., & Oelschläger, H. A. (2016). *Anatomy of dolphins: Insights into body structure and function* (p. 438). Amsterdam: Elsevier/Academic Press.
- Dammann, P., & Burda, H. (2006). Sexual activity and reproduction delay ageing in a mammal. *Current Biology*, 16(4), R117–R118.
- de Vries, J. L., Oosthuizen, M. K., Sichilima, A. M., & Bennett, N. C. (2008). Circadian rhythms of locomotor activity in Ansell's mole-rat: Are mole-rat's clocks ticking? *Journal of Zoology*, 276(4), 343–349.
- Ezure, K., & Tanaka, I. (1997). Convergence of central respiratory and locomotor rhythms onto single neurons of the lateral reticular nucleus. *Experimental Brain Research*, 113(2), 230–242.
- Garcia Montero, A., Burda, H., & Begall, S. (2015). Chemical restraint of African mole-rats (*Fukomys* sp.) with a combination of ketamine and xylazine. *Veterinary Anaesthesia and Analgesia*, 42, 187–191.
- Gerhardt, P., Henning, Y., Begall, S., & Malkemper, E. P. (2017). Audiograms of three subterranean rodent species (genus *Fukomys*) determined by auditory brainstem responses reveal extremely poor high-frequency cut-offs. *The Journal of Experimental Biology*, 220(23), 4377–4382.
- Gessele, N., Garcia-Pino, E., Omerbašić, D., Park, T. J., & Koch, U. (2016). Structural changes and lack of HCN1 channels in the binuclear auditory brainstem of the naked mole-rat (*Heterocephalus glaber*). *PLoS One*, 11(1), e0146428.
- Glendenning, K., & Masterton, R. (1998). Comparative morphometry of mammalian central auditory systems: Variation in nuclei and form of the ascending system. *Brain, Behavior and Evolution*, 51(2), 59–89.
- Godfrey, D. A., Lee, A. C., Hamilton, W. D., Benjamin, L. C., III, Vishwanath, S., Simo, H., ... Heffner, R. S. (2016). Volumes of cochlear nucleus regions in rodents. *Hearing Research*, 339, 161–174.
- Grothe, B., Pecka, M., & McAlpine, D. (2010). Mechanisms of sound localization in mammals. *Physiological Reviews*, 90(3), 983–1012.
- Heffner, R. S., & Heffner, H. E. (1990). Vestigial hearing in a fossorial mammal, the pocket gopher (*Geomys bursarius*). *Hearing Research*, 46, 239–252.
- Heffner, R. S., & Heffner, H. E. (1992). Hearing and sound localization in blind mole rats (*Spalax ehrenbergi*). *Hearing Research*, 62, 206–216.
- Heffner, R. S., & Heffner, H. E. (1993). Degenerate hearing and sound localization in naked mole rats (*Heterocephalus glaber*), with an overview of central auditory structures. *The Journal of Comparative Neurology*, 331(3), 418–433.
- Henry, E. C., Remple, M. S., O'Riain, M. J., & Catania, K. C. (2006). Organization of somatosensory cortical areas in the naked mole-rat (*Heterocephalus glaber*). *The Journal of Comparative Neurology*, 495(4), 434–452.
- Herculano-Houzel, S. (2009). The human brain in numbers: A linearly scaled-up primate brain. *Frontiers in Human Neuroscience*, 3(31), 1–11.
- Heth, G., Frankenberg, E., & Nevo, E. (1986). Adaptive optimal sound for vocal communication in tunnels of a subterranean mammal (*Spalax ehrenbergi*). *Experientia*, 42, 1287–1289.

- Heth, G., & Todrank, J. (2007). Using odors underground. In S. Begall, H. Burda, & C. E. Schleich (Eds.), *Subterranean rodents: News from underground* (pp. 85–96). Heidelberg: Springer.
- Heth, G., Todrank, J., Begall, S., Braude, S., Koch, R., Zilbiger, Y., ... Burda, H. (2002). Odour-guided foraging: “Blind” subterranean rodents do not search “blindly”. *Behavioral Ecology and Sociobiology*, 52, 53–58.
- Kalamatianos, T., Faulkes, C. G., Oosthuizen, M. K., Poorun, R., Bennett, N. C., & Coen, C. W. (2010). Telencephalic binding sites for oxytocin and social organization: A comparative study of eusocial naked mole-rats and solitary cape mole-rats. *The Journal of Comparative Neurology*, 518(10), 1792–1813.
- Kock, D., Ingram, C. M., Frabotta, L. J., Honeycutt, R. L., & Burda, H. (2006). On the nomenclature of Bathyergidae and *Fukomys* n. gen. (*Mammalia: Rodentia*). *Zootaxa*, 1142, 51–55.
- Kott, O., Némec, P., Fremlová, A., Mazoch, V., & Šumbera, R. (2016). Behavioural tests reveal severe visual deficits in the strictly subterranean African mole-rats (Bathyergidae) but efficient vision in the fossorial rodent coruro (*Spalacopus cyanus*, Octodontidae). *Ethology*, 122(8), 682–694.
- Kott, O., Šumbera, R., & Némec, P. (2010). Light perception in two strictly subterranean rodents: Life in the dark or blue? *PLoS One*, 5, e11810.
- Kruska, D. C., & Steffen, K. (2009). Encephalization of Bathyergidae and comparison of brain structure volumes between the Zambian mole-rat *Fukomys anselli* and the giant mole-rat *Fukomys mechowii*. *Mammalian Biology*, 74(4), 298–307.
- Kverková, K., Bělíková, T., Olkowicz, S., Pavelková, Z., O’Riain, M. J., Šumbera, R., ... Némec, P. (2018). Sociality does not drive the evolution of large brains in eusocial African mole-rats. *Scientific Reports*, 8(1), 9203.
- Lange, S., Burda, H., Wegner, R. E., Dammann, P., Begall, S., & Kawalika, M. (2007). Living in a “stethoscope”: Burrow-acoustics promote auditory specializations in subterranean rodents. *Naturwissenschaften*, 94(2), 134–138.
- Larson, J., & Park, T. J. (2009). Extreme hypoxia tolerance of naked mole-rat brain. *Neuroreport*, 20(18), 1634–1637.
- Malewski, S., Malkemper, E. P., Sedláček, F., Šumbera, R., Caspar, K. R., Burda, H., & Begall, S. (2018). Attracted by a magnet: Exploration behaviour of rodents in the presence of magnetic objects. *Behavioural Processes*, 151, 11–15.
- Malkemper, E. P., Oelschläger, H. H. A., & Huggenberger, S. (2012). The dolphin cochlear nucleus—Topography, histology and functional implications. *Journal of Morphology*, 273(2), 173–185.
- Malmierca, M. S. (2015). Auditory system. In G. Paxinos (Ed.), *The rat nervous system* (4th ed., pp. 865–946). Amsterdam: Elsevier.
- Marhold, S., Burda, H., Kreilos, I., & Wiltschko, W. (1997). *Magnetic orientation in common mole-rats from Zambia* (pp. 1–9). London: Oxford University, Royal Institute of Navigation.
- Marhold, S., Wiltschko, W., & Burda, H. (1997). A magnetic polarity compass for direction finding in a subterranean mammal. *Naturwissenschaften*, 84(9), 421–423.
- Mason, M., & Narins, P. (2010). Seismic sensitivity and communication in subterranean mammals. In C. E. O’Connell-Rodwell (Ed.), *The use of vibrations in communication: Properties, mechanisms and function across taxa* (pp. 121–139). Kerala: Transworld Research Network.
- Mason, M. J., Cornwall, H. L., & Smith, E. S. J. (2016). Ear structures of the naked mole-rat, *Heterocephalus glaber*, and its relatives (Rodentia: Bathyergidae). *PLoS One*, 11(12), e0167079.
- Monadjem, A., Taylor, P. J., Denys, C., & Cotterill, F. P. (2015). *Rodents of Sub-Saharan Africa: A Biogeographic and Taxonomic Synthesis*. Berlin, Boston: Walter de Gruyter GmbH & Co KG.
- Müller, M., & Burda, H. (1989). Restricted hearing range in a subterranean rodent, *Cryptomys hottentotus*. *Naturwissenschaften*, 76(3), 134–135.
- Müller, M., Laube, B., Burda, H., & Bruns, V. (1992). Structure and function of the cochlea in the African mole rat (*Cryptomys hottentotus*): Evidence for a low frequency acoustic fovea. *Journal of Comparative Physiology A: Neuroethology, Sensory, Neural, and Behavioral Physiology*, 171, 469–476.
- Némec, P., Altmann, J., Marhold, S., Burda, H., & Oelschläger, H. H. A. (2001). Neuroanatomy of magnetoreception: The superior colliculus involved in magnetic orientation in a mammal. *Science*, 294(5541), 366–368.
- Némec, P., Burda, H., & Peichl, L. (2004). Subcortical visual system of the African mole-rat *Cryptomys anselli*: To see or not to see? *The European Journal of Neuroscience*, 20(3), 757–758.
- Némec, P., Cvekova, P., Benada, O., Wielkopolska, E., Olkowicz, S., Turlejski, K., ... Peichl, L. (2008). The visual system in subterranean African mole-rats (Rodentia, Bathyergidae): Retina, subcortical visual nuclei and primary visual cortex. *Brain Research Bulletin*, 75, 356–364.
- Némec, P., Cveková, P., Burda, H., Benada, O., & Peichl, L. (2007). Visual systems and the role of vision in subterranean rodents: Diversity of retinal properties and visual system designs. In S. Begall, H. Burda, & C. Schleich (Eds.), *Subterranean rodents: News from underground* (pp. 129–160). Heidelberg: Springer.
- Nevo, E. (1999). *Mosaic Evolution of subterranean mammals: Regression, progression, and global convergence*. Oxford: Oxford University Press.
- Oelschläger, H. H. A. (2008). The dolphin brain—A challenge for synthetic neurobiology. *Brain Research Bulletin*, 75(2–4), 450–459.
- Oelschläger, H. H. A., Nakamura, M., Herzog, M., & Burda, H. (2000). Visual system labeled by c-Fos immunohistochemistry after light exposure in the ‘blind’ subterranean Zambian mole-rat (*Cryptomys anselli*). *Brain, Behavior and Evolution*, 55(4), 209–220.
- Oliveriusová, L., Némec, P., Králová, Z., & Sedláček, F. (2012). Magnetic compass orientation in two strictly subterranean rodents: Learned or species-specific innate directional preference? *The Journal of Experimental Biology*, 215(20), 3649–3654.
- Omerbašić, D., Smith, E. S. J., Moroni, M., Homfeld, J., Eigenbrod, O., Bennett, N. C., ... Lewin, G. R. (2016). Hypofunctional TrkA accounts for the absence of pain sensitization in the African naked mole-rat. *Cell Reports*, 17(3), 748–758.
- Osen, K. K. (1969). Cytoarchitecture of the cochlear nuclei in the cat. *The Journal of Comparative Neurology*, 136(4), 453–483.
- Park, T. J., Lu, Y., Jüttner, R., Smith, E. S. J., Hu, J., Brand, A., ... Heppenstall, P. A. (2008). Selective inflammatory pain insensitivity in the African naked mole-rat (*Heterocephalus glaber*). *PLoS Biology*, 6(1), e13.
- Park, T. J., Reznick, J., Peterson, B. L., Blass, G., Omerbašić, D., Bennett, N. C., ... Hamann, W. (2017). Fructose-driven glycolysis supports anoxia resistance in the naked mole-rat. *Science*, 356(6335), 307–311.
- Patterson, B. D., & Upham, N. S. (2014). A newly recognized family from the horn of Africa, the Heterocephalidae (Rodentia: Ctenohystrica). *Zoological Journal of the Linnean Society*, 172(4), 942–963.
- Patzenhauerová, H., Šklíba, J., Bryja, J., & Šumbera, R. (2013). Parentage analysis of Ansell’s mole-rat family groups indicates a high reproductive skew despite relatively relaxed ecological constraints on dispersal. *Molecular Ecology*, 22(19), 4988–5000.
- Paxinos, G. (2013). *Paxinos and Franklin’s the mouse brain in stereotaxic coordinates*. Boston: Elsevier/Academic Press.
- Paxinos, G., & Watson, C. (2013). *The rat brain in stereotaxic coordinates*. Boston: Elsevier/Academic Press.
- Peichl, L., Némec, P., & Burda, H. (2004). Unusual cone and rod properties in subterranean African mole-rats (Rodentia, Bathyergidae). *The European Journal of Neuroscience*, 19, 1545–1558.
- Peragine, D., Simpson, J., Mooney, S., Lovern, M., & Holmes, M. (2014). Social regulation of adult neurogenesis in a eusocial mammal. *Neuroscience*, 268, 10–20.
- Rosen, G., De Vries, G., Goldman, S., Goldman, B., & Forger, N. (2007). Distribution of vasopressin in the brain of the eusocial naked mole-rat. *The Journal of Comparative Neurology*, 500(6), 1093–1105.
- Scharff, A., & Grütjen, O. (1997). Evidence for aboveground activity of Zambian Molerats (*Cryptomys*, Bathyergidae, Rodentia). *Mammalian Biology*, 62(4), 253–254.
- Sherman, P. W., Jarvis, J. U., & Alexander, R. D. (2017). *The biology of the naked mole-rat*. Princeton, NJ: Princeton University Press.
- Šklíba, J., Mazoch, V., Patzenhauerová, H., Hrouzková, E., Lövy, M., Kott, O., & Šumbera, R. (2012). A maze-lover’s dream: Burrow architecture, natural history and habitat characteristics of Ansell’s mole-rat (*Fukomys anselli*). *Mammalian Biology*, 77(6), 420–427.
- Sugiyō, S., Takemura, M., Dubner, R., & Ren, K. (2006). Demonstration of a trigeminothalamic pathway to the oval paracentral intralaminar thalamic nucleus and its involvement in the processing of noxious orofacial deep inputs. *Brain Research*, 1097(1), 116–122.
- Swanson, L. (2004). *Brain maps: Structure of the rat brain. An atlas with printed and electronic templates for data, models, and schematics*. Amsterdam: Elsevier.
- Thalau, P., Ritz, T., Burda, H., Wegner, R. E., & Wiltschko, R. (2006). The magnetic compass mechanisms of birds and rodents are based on

- different physical principles. *Journal of the Royal Society Interface*, 3(9), 583–587.
- Valesky, E. M., Burda, H., Kaufmann, R., & Oelschläger, H. H. A. (2012). Distribution of oxytocin- and vasopressin-immunoreactive neurons in the brain of the eusocial mole-rat (*Fukomys anselli*). *The Anatomical Record*, 295(3), 474–480.
- Van Daele, P., Herrel, A., & Adriaens, D. (2008). Biting performance in teeth-digging African mole-rats (*Fukomys*, Bathyergidae, Rodentia). *Physiological and Biochemical Zoology*, 82(1), 40–50.
- Wegner, R. E., Begall, S., & Burda, H. (2006a). Light perception in 'blind' subterranean Zambian mole-rats. *Animal Behaviour*, 72(5), 1021–1025.
- Wegner, R. E., Begall, S., & Burda, H. (2006b). Magnetic compass in the cornea: Local anaesthesia impairs orientation in a mammal. *The Journal of Experimental Biology*, 209(23), 4747–4750.
- Wilson, D. E., Mittermeier, R. A., Ruff, S., Martínez-Vilalta, A., & Cavallini, P. (2016). *Handbook of the mammals of the world: Lagomorphs and rodents I*. Bellaterra: Lynx Edicions.
- Xiao, J., Levitt, J., & Buffenstein, R. (2006). A stereotaxic atlas of the brain of the naked mole-rat (*Heterocephalus glaber*). *Neuroscience*, 141(3), 1415–1435.
- Young, E. D., & Davis, K. A. (2002). Circuitry and function of the dorsal cochlear nucleus. In D. Oertel, R. R. Fay, & A. N. Popper (Eds.), *Integrative functions in the mammalian auditory pathway* (pp. 160–206). New York, NY: Springer.

How to cite this article: Dollas A, Oelschläger HHA, Begall S, Burda H, Malkemper EP. Brain atlas of the African mole-rat *Fukomys anselli*. *J Comp Neurol*. 2019;527:1885–1900. <https://doi.org/10.1002/cne.24647>